

¹ Drought indices of water demand and supply, soil moisture, vegetation, and
² their impact on LULCC in continental Chile

³ Francisco Zambrano^{a,1,*}

^a Universidad Mayor, Hémera Centro de Observación de la Tierra, Facultad de Ciencias, Escuela de Ingeniería en Medio Ambiente y Sustentabilidad, Santiago, Chile, 7500994

⁴ **Abstract**

Central Chile has been the focus of research studies due to the persistent decrease in water supply, which is impacting the hydrological system and vegetation development. This persistent period of water scarcity has been defined as a “Mega Drought”. Our objective is to examine the effects of drought on LULCC (land use land cover change) over continental Chile using drought indices of water supply and demand, soil moisture, and vegetation productivity. For the analysis, continental Chile was divided into five zones according to a latitudinal gradient: “Norte Grande,” “Norte Chico,” “Centro,” “Sur,” and “Austral.” The monthly ERA5-Land (ERA5L) variables for precipitation, temperature, and soil moisture were used. From 2001 to 2022, we used the land cover MODIS product MCD12Q1, and from 2000 to 2023, we used the NDVI (Normalized Difference Vegetation Index) product MOD13A3 collection 6.1. We estimated atmospheric evaporative demand (AED) using the Hargreaves-Samani equation with the ERA5L temperature. We used the Standardized Precipitation Index (SPI), the Standardized Precipitation Evapotranspiration Index (SPEI), the Evaporative Demand Drought Index (EDDI), the Standardized Soil Moisture Index (SSI), and the Standardized anomaly of cumulative NDVI (zcNDVI) as drought indicators. These indices were calculated for time scales of 1, 3, 6, 12, 24, and 36 months, except for zcNDVI, which was for 6 months. We analyze the trend for LULCC, vegetation productivity, and drought indices. Also, we analyzed the temporal correlation of SPI, SPEI, EDDI, and SSI with zcNDVI to gain insights into the impact of water supply and demand on vegetation productivity. Our results showed that LULCC were highest in “Centro,” “Sur,” and “Austral,” with 36%, 31%, and 34%, respectively. The EDDI shows that water demand has increased for all zones, with a major increase in “Norte Grande.” The drought indices of water supply and soil moisture evidence a decreasing trend, which decreases at longer time scales, from “Norte Grande” to “Sur.” “Austral” is the only zone that shows an increase in supply. Vegetation productivity measures by zcNDVI present a negative trend in “Norte Chico” and “Centro.” Showing to be the zones most impacted by climatic conditions, the years 2020 and 2022 suffered the most extreme drought. On the other hand, forests seem to be the most resistant to drought. The types that show to be most affected by variation in climate conditions are shrublands, savannas, and croplands. The drought indices that have the capability of explaining to a major degree the variance in vegetation productivity are SSI-12, followed by SPEI-24 and SPEI-12 in “Norte Chico” and “Centro.” The results indicate that “Norte Chico” and “Zona Central” are the most sensitive regions to water supply deficits longer than a year, potentially explained by a low capacity of water storage in those zones that should be further investigated.

⁵ **Keywords:** drought, land cover change, satellite

*Corresponding author

Email address: francisco.zambrano@umayor.cl (Francisco Zambrano)

¹This is the first author footnote.

6 **1. Introduction**

7 The sixth assessment report (AR6) of the IPCC (Calvin et al., 2023) indicates that human-induced green-
8 house gas emissions have increased the frequency and/or intensity of some weather and climate extremes,
9 and the evidence has been strengthened since AR5 (IPCC, 2013). There is a high degree of confidence
10 that rising temperatures will increase the land area where droughts will occur more frequently and with
11 greater severity (Seneviratne, 2021). Furthermore, drought increases tree mortality and triggers changes in
12 land cover and, consequently, land use, thus impacting ecosystems (Crausbay et al., 2017). Nevertheless,
13 there is a lack of understanding of how the alteration in water supply and demand is affecting land cover
14 transformations.

15 The primary cause of drought is precipitation, and temperature makes it worse (Luo et al., 2017). Drought
16 impacts soil moisture, hydrological regimes, and vegetation productivity. Initially, drought was commonly
17 classified as meteorological, hydrological, and agricultural (Wilhite and Glantz, 1985). Lately, Van Loon
18 et al. (2016) and AghaKouchak et al. (2021) have given an updated definition of drought for the Anthro-
19 pocene, suggesting that it should be considered the feedback of humans' decisions and activities that drives
20 the anthropogenic drought. Even though it has been argued that those definitions do not fully address
21 the ecological dimensions of drought, Crausbay et al. (2017) proposed the ecological drought definition as
22 "an episodic deficit in water availability that drives ecosystems beyond thresholds of vulnerability, impacts
23 ecosystem services, and triggers feedback in natural and/or human systems." Moreover, many ecological
24 studies have misinterpreted how to characterize drought, for example, sometimes considering "dry" condi-
25 tions as "drought" (Slette et al., 2019). On the other hand, the AR6 (Calvin et al., 2023) predicts that many
26 regions of the world will experience more severe agricultural and ecological droughts even if global warming
27 stabilizes at 1.5°–2°C. Then, there is a challenge in conducting drought research, especially to evaluate its
28 impact on ecosystems.

29 Chile has been facing a persistent rainfall deficit for more than a decade (Garreaud et al., 2017), which
30 has impacted vegetation development (Zambrano, 2023) and the hydrological system (Boisier et al., 2018).
31 Current drought conditions have affected crop productivity (Zambrano et al., 2016, 2018), forest development
32 (Miranda et al., 2020; Venegas-González et al., 2018), forest fire occurrence (Urrutia-Jalabert et al., 2018),
33 land cover change (Fuentes et al., 2021), water supply in watersheds (Alvarez-Garreton et al., 2021), and
34 have had economic impacts (Fernández et al., 2023). In 2019–2020, the drought severity reached an extreme
35 condition in Central Chile (30–34°S) not seen for at least 40 years, and the evidence indicates that the
36 impact is transversal to the land cover classes of forest, grassland, and cropland (Zambrano, 2023). The
37 prolonged lack of precipitation in Central Chile is producing changes in ecosystem dynamics that must be
38 studied.

39 For the spatiotemporal assessment of drought impact (i.e., by water supply and demand) on land cover
40 changes, we need climatic reliable variables such as precipitation, temperature, soil moisture, land cover, and
41 vegetation status. For developing countries like Chile, the weather networks present several disadvantages,
42 such as gaps, a short history, and low-quality data. Reanalysis data, as the ERA5-Land (ERA5L) (Muñoz-
43 Sabater et al., 2021) provides hourly climatic information (precipitation, temperature, and soil moisture)
44 without gaps since 1950 with global extension. ERA5L has already been used for drought assessment using
45 the Standardized Precipitation-Evapotranspiration Index (SPEI) (Nouri, 2023) and for flash drought (Wang
46 et al., 2023) by analyzing soil moisture and evapotranspiration. On the other hand, satellite remote sensing
47 (West et al., 2019; AghaKouchak et al., 2015) is the primary method to evaluate how drought impacts
48 vegetation dynamics. The Moderate-Resolution Imaging Spectroradiometer (MODIS) can be used to get
49 vegetation drought indices (VDI), which are often used as proxies for productivity (Paruelo et al., 2016;
50 Schucknecht et al., 2017). Besides, land use and land cover (LULC) change can be driven by drought (Tran
51 et al., 2019; Akinyemi, 2021). To analyze these changes, multiple LULC products exist (Grekousis et al.,
52 2015). One of those that provides time series since 2001 is the MCD12Q1 (Friedl and Sulla-Menashe, 2019)
53 from MODIS. The variation in water supply and demand is finally reflected in the total water storage
54 (TWS). The Gravity Recovery and Climate Experiment (GRACE), which allows analyzing changes in water

55 availability at coarse resolution, can retrieve the TWS (Ahmed et al., 2014; Ma et al., 2017). We can
56 find drought indices of supply (i.e., precipitation) and demand (i.e., temperature) using climatic reanalysis
57 (ERA5L) and vegetation data (MODIS). This lets us figure out how drought changes LULC. Further, the
58 TWS can be assessed with regard to the changes in water supply and demand to gain insight into the impact
59 on water storage.

60 To evaluate meteorological drought (i.e., water supply), the World Meteorological Organization (WMO;
61 WMO et al. (2012)) recommends the Standardized Precipitation Index (SPI; McKee et al. (1993)), a multi-
62 scalar drought index that allows to monitor precipitation deficits from short- to long-term. Following the
63 same approach, Vicente-Serrano et al. (2010) incorporates into the SPI the effect of temperature through
64 the use of potential evapotranspiration, thus proposing the SPEI (Standardized Precipitation Evapotranspi-
65 ration Index). Similarly, to evaluate solely the evaporative demand driven by temperature, Hobbins et al.
66 (2016) and McEvoy et al. (2016) came up with the Evaporative Demand Drought Index (EDDI). For veg-
67 etation, in a similar manner as the SPI, SPEI and EDDI; Zambrano et al. (2018) proposed the zcNDVI,
68 a standardized anomaly of the cumulative Normalized Difference Vegetation Index (NDVI), which could
69 be accumulated over the growing season or any period (e.g., months), resulting in a multiscalar drought
70 index. For soil moisture, several drought indices exist, such as the Soil Moisture Deficit Index (SDMI) a
71 normalized index (Narasimhan and Srinivasan, 2005) and the Soil Moisture Agricultural Drought Index
72 (SMADI) (Souza et al., 2021) which is a normalized index using vegetation, land surface temperature, and a
73 vegetation condition index (VCI, (Kogan, 1995)). From TWS, we can estimate the standardized terrestrial
74 water storage index (STI) (Cui et al., 2021), a standardized anomaly that follows the methodology of the
75 SPI, SPEI, EDDI, and zcNDVI. Thereby, we have drought indices for water supply, demand, and storage,
76 which can help to make a comprehensive assessment of drought.

77 In this research, we aim to analyze the impact of drought on different types of ecosystems (land cover
78 classes) in continental Chile. Our specific goals are: i) to analyze the trend on multi-scalar drought indices
79 for water demand and supply, soil moisture, and vegetation productivity for 1981–2023/2001–2023; ii) to
80 assess the LULC change for 2001–2021 and how it relates to drought indices; iii) to evaluate the relationship
81 between zcNDVI, a measure of vegetation productivity, and drought indices for water demand and supply
82 and soil moisture; and iv) to assess if the observed changes in the drought indices are linked to TWS.

83 2. Study area

84 Continetal Chile has a diverse climate condition from north to south and east to west (Aceituno et al.,
85 2021) (Figure 1), which determines its great ecosystem diversity (Figure 2). The Andes Mountains are a
86 main factor in latitudinal variation (Garreaud, 2009). To describe the climate and ecosystem of Chile, we
87 use the Koppen-Geiger release by Beck et al. (2023) and the land cover type persistance of 80% of times
88 for 2001–2022, from the IGBP classification scheme (Friedl and Sulla-Menashe, 2019) (see Section 3.4).
89 “Norte Grande” and “Norte Chico” predominate in an arid desert climate with hot (Bwh) and cold (Bwk)
90 temperatures. At the south of “Norte Chico,” the climate changes to an arid steppe with cold temperatures
91 (Bsk). Mainly, the land is barren, with a minor surface of vegetation types such as shrubland and grassland.
92 In the zones “Centro” and the north half of “Sur,” the main climate is Mediterranean, with warmer to hot
93 summers (Csa and Csb). There is a significant amount (50%) of Chilean matorral (shrubland and savanna,
94 (Fuentes et al., 2021)), then grassland (16%), forest (8%), and croplands (5%), in “Centro.” The south part
95 of “Sur” and the north part of “Austral” are dominated by an oceanic climate (Cfb). Those zones are high
96 in forest and grassland. The southern part of the country has a tundra climate, and in Patagonia, it is a
97 cold semi-arid area with an extended surface of grassland, forest, and, to a lesser extent, savanna.

98 3. Materials and Methods

99 3.1. Software and packages used

100 For the downloading, processing, and analysis of the spatio-temporal data, we used the open source software
101 for statistical computing and graphics, R (R Core Team, 2023). For downloading ERA5L, we used the

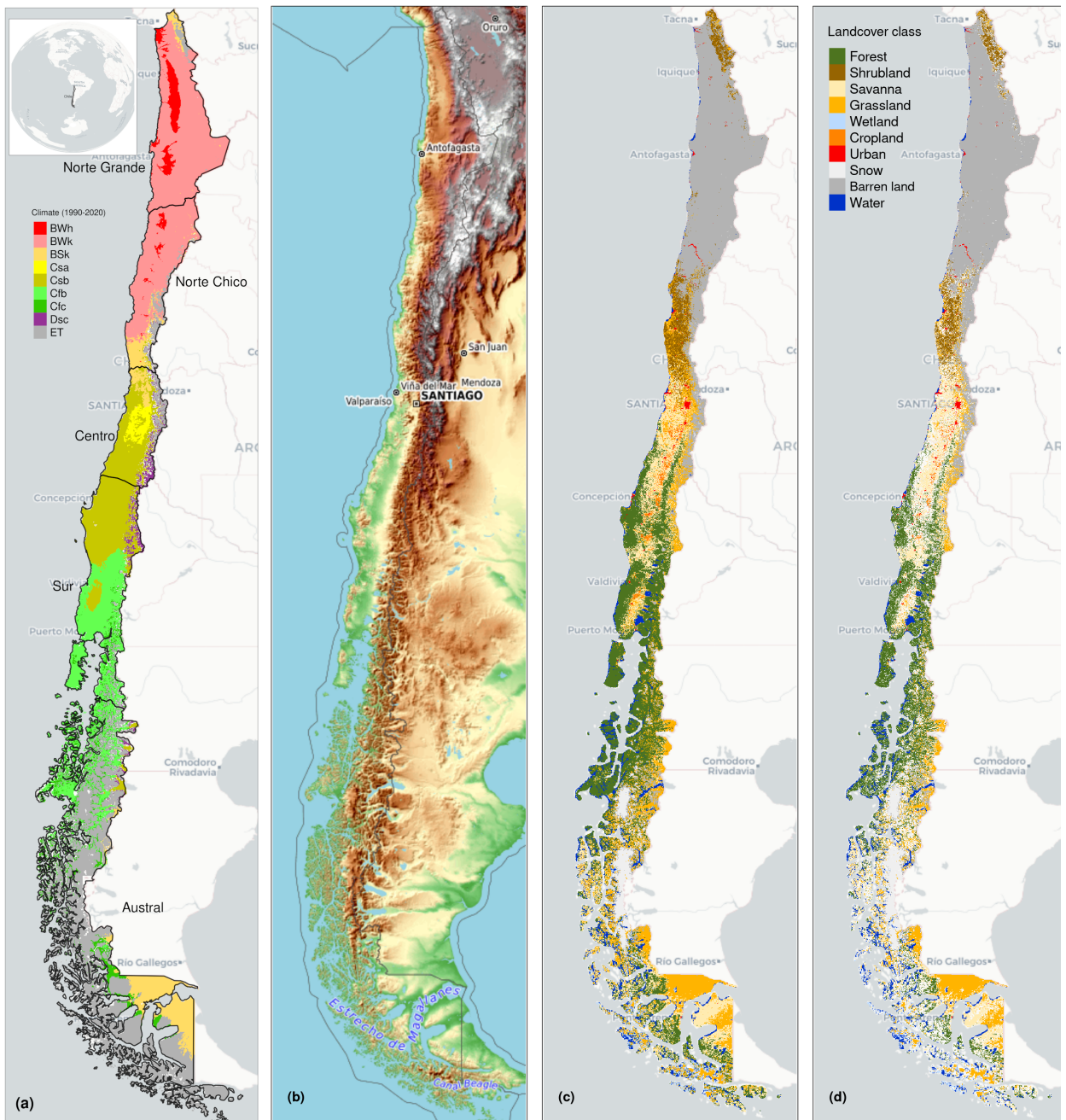


Figure 1: (a) Chile with the Koppen-Geiger climate classes and the five macrozones “Norte Grande”, “Norte Chico”, “Centro”, “Sur”, and “Austral”. (b) Topography reference map. (c) Land cover classes for 2022. (d) Persistent land cover classes (> 80%) for 2001-2022

102 {ecmwfr} package (Hufkens et al., 2019). For processing raster data, we used {terra} (Hijmans, 2023) and
 103 {stars} (Pebesma and Bivand, 2023). For managing vectorial data, we used {sf} (Pebesma, 2018). For
 104 the calculation of AED, we used {SPEI} (Beguería and Vicente-Serrano, 2023).

105 *3.2. Data*

106 *3.2.1. Earth observation data*

107 For water supply and demand variables, we used ERA5L ([Muñoz-Sabater et al., 2021](#)), a reanalysis dataset
108 that provides the evolution of land variables since 1950. It has a spatial resolution of 0.1° , hourly frequency,
109 and global coverage. We selected the variables for total precipitation, 2 meter temperature maximum and
110 minimum, and volumetric soil water layers between 0 and 100cm of depth (layer 1 to layer 3). The data
111 was downloaded using the Copernicus Climate Data Store (CDS) Application Program Interface (API)
112 implemented in `{ecmfwr}` ([Hufkens et al., 2019](#)).

113 To derive a proxy of vegetation productivity, we used the product MOD13A3 collection 6.1 from MODIS
114 ([Didan, 2015](#)). It provides vegetation indices (NDVI and EVI) at 1km of spatial resolution and monthly
115 frequency. The MOD13A3.061 and MCD12Q1.061 were retrieved from the online Data Pool, courtesy of
116 the NASA EOSDIS Land Processes Distributed Active Archive Center (LP DAAC), USGS Earth Resources
117 Observation and Science (EROS) Center, Sioux Falls, South Dakota, <https://lpdaac.usgs.gov/tools/data-pool/>.

Table 1: Description of the earth observation data used

Product	Sub-product	Variable	Spatial Resolution	Period	Units	Short Name	
ERA5L		Precipitation	0.1°	1981-2023	mm	P	
		Maximum temperature			$^\circ C$	T_{max}	
		Minimum temperature			$^\circ C$	T_{min}	
		Volumetric Soil Water Content at 1m			m^3/m^3	SM	
ERA5L*	MODIS	Atmospheric Evaporative Demand	0.1°	1981-2023	mm	AED	
MODIS		Normalized Difference Vegetation Index	1 km	2000-2023		NDVI	
		land cover IGBP scheme		2001-2022		land cover	

*Derived from ERA5L with Eq. 1.

119 *3.2.2. Weather stations*

120 We compared the ERA5L variables for monthly mean temperature, total precipitation, and volumetric soil
121 water content against values retrieved by weather stations. For temperature and precipitation, we used the
122 weather network from the Ministry of Agriculture of Chile (www.agromet.com) between 2015 and 2023. We
123 used 277 stations located throughout Chile. For soil moisture, we select a private soil network that is owned
124 by the agricultural enterprise Garces Fruit, which has 99 stations in Central Chile, located in cherry fruit
125 crops. We used daily data for the year 2022 and the months outside the growing season, May to September,
126 to avoid the effect of irrigation on soil moisture, which is hardly captured by ERA5L.

127 *3.2.3. Validation of ERA5L variables*

128 To account for the performance of the ERA5L climatic variables regarding the values measured by the
129 weather stations. We selected the following metrics:

$$MAE = \frac{1}{n} \sum |E - S|$$

$$Bias = \frac{\sum E}{\sum S}$$

$$ubRMSE = \sqrt{\frac{\sum [(E_i - \bar{E}) - (S_i - \bar{S})]^2}{n}}$$

$$CC = \frac{\sum(S_i - \bar{S})(E_i - \bar{E})}{\sqrt{(S_i - \bar{S})^2(E_i - \bar{E})^2}}$$

132 *MAE*: mean absolute error *bias*: bias *ubRMSE*: unbiased root mean squared error *CC*: coefficient of
 133 correlation *S*: value of the variable measure by the weather station *E*: value of the variable measure by
 134 ERA5L

135 *3.3. Drought Indices*

136 *3.3.1. Atmospheric Evaporative Demand (AED)*

137 For the indices EDDI and SPEI that use water demand, first we have to calculate the AED. For this, we
 138 used the method of Hargreaves ([Hargreaves, 1994](#); [Hargreaves and Samani, 1985](#)):

$$AED = 0.0023 \cdot Ra \cdot (T + 17.8) \cdot (T_{max} - T_{min})^{0.5} \quad (1)$$

139 where *Ra* ($MJ m^2 day^{-1}$) is extraterrestrial radiation; *T*, *T_{max}*, and *T_{min}* are mean, maximum, and
 140 minimum temperature ($^{\circ}C$). We calculate the centroid coordinates per pixel and use the latitude to estimate
 141 *Ra*.

142 We chose the method of Hargreaves to estimate AED because of its simplicity, which only requires tem-
 143 peratures and extrarrestrial radiation. Also, it has been recommended over other methods when the use of
 144 several climatic variables is limited ([Vicente-Serrano et al., 2014](#)).

145 *3.3.2. Non-parametric calculation of drought indices*

146 We derived the drought indices of water supply and demand, soil moisture from the ERA5L dataset, and
 147 vegetation from the MODIS product, all at monthly frequency.

148 To evaluate water demand, we chose the *EDDI* ([Hobbins et al., 2016](#); [McEvoy et al., 2016](#)) index, which
 149 uses the *AED*. For supply, we used the index recommended by the World Meteorological Organization
 150 (WMO) for monitoring drought, the *SPI* ([McKee et al., 1993](#)). We calculated the *SPEI*, which used a
 151 balance between *P* and *AED*, in this case, an auxiliary variable *D* = *P* − *AED* is used. In this study,
 152 we used the *SSI* (standardized soil moisture index at 1 m) ([Hao and AghaKouchak, 2013](#); [AghaKouchak,
 153 2014](#)), which uses soil moisture at 1m depth. Finally, for the proxy of productivity, *zcNDVI*, we used the
 154 *NDVI*. Before using the *NDVI*, it was smoothed using a locally-weighted polynomial regression, following
 155 the procedure described in [Zambrano et al. \(2018\)](#) and [Zambrano et al. \(2016\)](#).

156 All the indices are multi-scalar and were calculated for time scales of 1, 3, 6, 12, 24, and 36 months, except
 157 for *zcNDVI*, which was calculated for 6 months. The goal is to be able to evaluate short- and long-term
 158 droughts in water demand and supply and soil moisture. This is particularly important for central Chile
 159 because it has suffered from a prolonged decrease in precipitation for more than 12 years ([Garreaud et al.,
 160 2020](#); [Boisier et al., 2018](#); [Garreaud et al., 2017](#)).

161 To calculate the drought indices, first we must calculate the accumulation of the variable. In this case, for
 162 generalization purposes, we will use *V*, referring to *P*, *AED*, *D*, *NDVI*, and *SM* (Table 1). We cumulated
 163 each *V* over the time series of *n* values, and for the time scales *s*:

$$A_{si} = \sum_{i=n-s-i+2}^{n-i+1} V_i \quad \forall i \geq n - s + 1 \quad (2)$$

164 It corresponds to a moving window (convolution) that sums the variable for *s* starting for the last month
 165 *n* until the month, which could sum for *s* months (*n*-*s*+1). Once the variable is cumulated over time

for the scale s , we used a nonparametric approach following Hobbins et al. (2016) to derive the drought indices. Thus, the empirically derived probabilities are obtained through an inverse normal approximation (Abramowitz and Stegun, 1968). Then, we used the empirical Tukey plotting position (Wilks, 2011) over A_i to derive the $P(A_i)$ probabilities across a period of interest:

$$P(A_i) = \frac{i - 0.33}{n + 0.33} \quad (3)$$

The drought indices *SPI*, *SPEI*, *EDDI*, *SSI*, and *zcNDVI* are obtained following the inverse normal approximation:

$$DI(A_i) = W - \frac{C_0 + C_1 \cdot W + c_2 \cdot W^2}{1 + d_1 \cdot W + d_2 \cdot W^2 + d_3 \cdot W^3} \quad (4)$$

DI is referring to the drought index calculated for the variable V . The values for the constants are: $C_0 = 2.515517$, $C_1 = 0.802853$, $C_2 = 0.010328$, $d_1 = 1.432788$, $d_2 = 0.189269$, and $d_3 = 0.001308$. For $P(A) \leq 0.5$, $W = \sqrt{-2 \cdot \ln(P(A_i))}$, and for $P(A_i) > 0.5$, replace $P(A_i)$ with $1 - P(A_i)$ and reverse the sign of $DI(A_i)$.

3.4. LULC change for 2001-2022 and its relation with water supply and demand, and soil moisture

3.4.1. land cover macroclasses and validation

To analyze the LULCC, we use the IGBP scheme from the MCD12Q1 collection 6.1 from MODIS. This product has a yearly frequency from 2001 to 2022. The IGBP defines 17 classes; from these, we regrouped into ten macroclasses, as follows: classes 1-4 to forest, 5-7 to shrublands, 8-9 to savannas, 10 as grasslands, 11 as wetlands, 12 and 14 to croplands, 13 as urban, 15 as snow and ice, 16 as barren, and 17 to water bodies. Thus, we have a land cover raster time-series with the ten classes for 2001 and 2023.

To validate the land cover obtained, we compare the macroclasses with the ones of a more detailed land cover map made by Zhao et al. (2016) for Chile with samples acquired in the years 2013–2014 (LCChile). The latter has a spatial resolution of 30 m and three levels of defined classes; from those, we used level 1, which fits with the macroclasses land cover. We chose the years 2013 (IGBP2013) and 2014 (IGBP2014) from land cover macrolcasses to validate with LCChile.

We follow the next procedure:

- i) resampled LCChile to the spatial resolution (500m) of the land cover macroclasses using the nearest neighbor method,
- ii) took a random sample of 1000 points within continental Chile and extracted the classes that fell within each point for LCChile, IGBP2013, and IGBP2014; we considered the point extracted from LCChile as the truth and the values as the other two years as prediction
- iii) calculate a confusion matrix with the classes extracted in the 1000 poitns for LCChile, IGBP2013, and IGBP2014. Calculate the performance metrics of accuracy and F1.

$$Accuracy = \frac{TP + TN}{TP + TN + FP + FN} = \frac{\text{correct classifications}}{\text{all classifications}}$$

$$F1 = \frac{2 \cdot TP}{2 \cdot TP + FP + FN}$$

where TP and FN refer to true positive and false negative, correctly classified classes; TN and FP to true negative and false positive, wrongly classified classes.

199 *3.4.2. land cover persistence mask 2001–2022*

200 The time series of NDVI is affected by climatic conditions, vegetation development, seasonality, and changes
201 in vegetation type. In this study, we want to analyze the variation in vegetation productivity in different
202 land cover types and how it is affected by water demand, water supply, and soil moisture. In order to
203 avoid changes due to a change in the land cover type, that will wrongly impact NDVI. We will develop a
204 persistence mask for land cover for 2001–2023. Thereby, we reduce an important source of variation on a
205 regional scale.

206 Thus, we calculated a raster mask for IGBP MODIS considering the macroclasses that remain without
207 change for more than 80% of the years (2001–2022) per pixel, which allows us to identify the areas with no
208 land cover change for the macroclasses.

209 *3.4.3. land cover trend and drought indices*

210 We calculated the surface occupied per land cover class into the five macrozones (“Norte Grande” to
211 “Austral”) per year for 2001–2023. After that, we calculated the trend’s change in surface; we used the Sen’
212 slope (Sen, 1968) based on Mann-Kendall (Kendall, 1975). This way, we obtain a matrix of trends of 5 x 5
213 (macrozones x land cover). The aim is to later explore if the trend in land cover classes is associated with
214 a trend in the drought indices. For this, we will use the techniques of regresion and regularization of Lasso
215 (Tibshirani et al., 2010) and Ridge (Hoerl and Kennard, 1970). Also, we will test random forests for this
216 purpose (Ho, 1995). We will choose the trend of land cover surface per macroclass and macrozone as the
217 response variable and the trend of the drought indices (SPI, SPEI, EDDI, and SSI for time scales 1, 3, 6, 12,
218 24, and 36 months) as the predictor variables. With this analysis, we expect to gather insights regarding
219 whether there is a pattern of climatic influence along Chile or if what is happening in Central Chile has to
220 do with more localized climatic conditions.

221 *3.5. Trend of drought indices for water demand and supply, soil moisture, and vegetation productivity*

222 *3.5.1. Mann-Kendall and Sen’s slope*

223 To estimate if there are significant positive or negative trends for the drought indices, we used the non-
224 parametric test of Mann-Kendall (Kendall, 1975). To determine the magnitude of the trend, we used Sen’s
225 slope (Sen, 1968). Some of the advantages of applying this methodology are that the Sen’s slope is not
226 affected by outliers as regular regression does, and it is a non-paramteric method that is not affected by the
227 distribution of the data. We applied both to the six time scales from 1981 to 2023 (monthly frequency) and
228 the indices SPI, EDDI, SPEI, and SSI. In the case of zcNDVI (six months) was for 2000 to 2023. Thus, we
229 have 31 trends. Also, we extracted the trend aggregated by macrozone and land cover class, obtaining a
230 table of 31x5x5 (drought indices trends x macrozone x land cover class). We will use this data in Section 3.4
231 to analyze if there is a strong relationship between the trends of drought indices and land cover surface
232 within continental Chile.

233 *3.5.2. Trend in vegetation productivity without land cover change*

234 Vicente-Serrano et al. (2022) made a global analysis of the drought’s severity trend using SPI, SPEI, and
235 the Standardized Evapotranspiration Deficit Index (SEDI; Vicente-Serrano et al. (2018)) to evaluate AED.
236 They indicate that the increase in hydrological drought has been due to anthropogenic effects rather than
237 climate change. This is because the global increase in AED did not explain the change in the spatial pattern
238 of the hydrological drought. Also, they state that “*the increase in hydrological droughts has been primarily*
239 *observed in regions with high water demand and land cover change*”. We will contrast this hypothesis with
240 what is occurring in Chile. To achieve this, we will use the land cover class type that remains more than
241 80% of types for 2001–2022 to evaluate the trend on zcNDVI and use this as a mask where there are low
242 changes.

243 *3.6. Impact for water supply and demand, and soil moisture in vegetation productivity within land cover*
244 *types*

245 We analyze the drought indices of water demand and supply and soil moisture against vegetation to address:
246 i) if short- or long-term time scales are most important in impacting vegetation through Chile; and ii) the

strength of the correlation for the variable and the time scale. Then, we will summarize for each land cover class and macrozone. Thus, we will be able to advance in understanding how climate is affecting vegetation, considering the impact on the five macroclasses having vegetation: forest, cropland, grassland, savanna, and shrubland.

To assess how water demand and supply and soil moisture are related to vegetation productivity (zcNDVI), we analyze the linear correlation between the indices SPI, SPEI, EDDI, and SSI for 1, 3, 6, 12, 24, and 36-month time scales against zcNDVI. We followed a similar approach to that used by Meroni et al. (2017) when using the SPI for meteorological drought against the cumulative FAPAR (Fraction of Absorbed Photosynthetically Active Radiation) as a proxy for vegetation productivity. We made a pixel-to-pixel linear correlation analysis per index. First, we calculate the Pearson coefficient of correlation for the six time scales and let the time scale that reaches the maximum correlation be significant ($p < 0.05$). Then, we extracted the Pearson correlation value corresponding to the time scales that reached the maximum value. Thus, we derived two raster maps per index, the first with the time scales and the second with the correlation value.

4. Results

4.1. Data

4.1.1. Validation of ERA5L variables

The average metrics of performance of ERA5L over the 266 weather stations were in the case of monthly temperature: $ubRMSE = 1.06^{\circ}\text{C}$, $MAE = 1.131^{\circ}\text{C}$, and $CC = 0.963$, showing a good agreement, low error, and low overestimation. For cumulative monthly precipitation, $MAE = 28.1 \text{ mm}$, $bias = 1.93$, and $CC = 0.845$, showing a high correlation and a 93% bias and being overestimated by ERA5L. In the case of the 97 soil moisture stations, we averaged for the three depths (30, 60, and 90m) and then compared it with volumetric water content at 1m derived from ERA5L. For this case, we made a daily comparison, having a $CC = 0.71$, $RMSE = 0.174 \text{ m}^3\text{m}^{-3}$, $MAE = 0.167 \text{ m}^3\text{m}^{-3}$, and $bias = 1.74$. The ERA5 soil moisture overestimate is 74%, but it has a kind of good correlation.

4.2. LULC change for 2001-2022 and its relation with water supply and demand, and soil moisture

4.2.1. land cover macroclases and validation

For vegetation, we obtained and use hereafter five macroclasses of land cover from IGBP MODIS: forest, shrubland, savanna, grassland, and croplands. Figure 1 c shows the spatial distribution of the macroclasses through Chile for the year 2022. The validation of IGBP2013 and IGBP2014 with LCChile reached near the same metrics of performance, having an accuracy of ~ 0.82 and a F1 score of ~ 0.66 (see SS1).

4.2.2. land cover persistence mask 2001-2022

Figure 1 d, shows the macroclasses of land cover persistence (80%) during 2021-2022, respectively. Within continental Chile, forest is the vegetation type with highest surface with $135,00 \text{ km}^2$, followed by grassland ($73,176 \text{ km}^2$), savanna ($54,410 \text{ km}^2$), shrubland ($24,959 \text{ km}^2$), and cropland ($3,100 \text{ km}^2$) (2). The macrozones with major LULCC for 2001-2022 were “Centro”, “Sur”, and “Austral” with 36%, 31%, and 34%, respectively (Figure 1 and Table 3); of its surface that changes the type of land cover. Figure 2 shows the summary of the proportion of surface per land cover class and macrozone, derived from the persistence mask over continental Chile.

4.2.3. land cover trend and drought indices

The “Norte Chico” shows an increase in barrend land of $111 \text{ km}^2\text{year}^{-1}$ and a reduction in the class savanna of $70 \text{ km}^2\text{year}^{-1}$. In the “Centro” and “Sur,” there are changes in the Chilean matorral, with an important reduction in savanna (136 to $318 \text{ km}^2\text{yr}^{-1}$), and an increase in shrubland and grassland. Showing a change for more dense vegetation types. It appears to be a shift in the area of cropland from the “Centro” to the “Sur.” Also, there is a high increase in forest ($397 \text{ km}^2\text{yr}^{-1}$) in the “Sur,” replacing the savanna lost.

Table 2: Surface of the land cover class that persist during 2001-2022

macrozone	Surface [km ²]					
	Forest	Cropland	Grassland	Savanna	Shrubland	Barren land
Norte Grande		873		7,796		169,244
Norte Chico		88	4,221	580	16,085	83,059
Centro	3,685	1,876	7,475	19,420	832	12,304
Sur	71,943	1,135	7,094	15,676		2,143
Austral	59,481		53,514	18,733	245	7,114

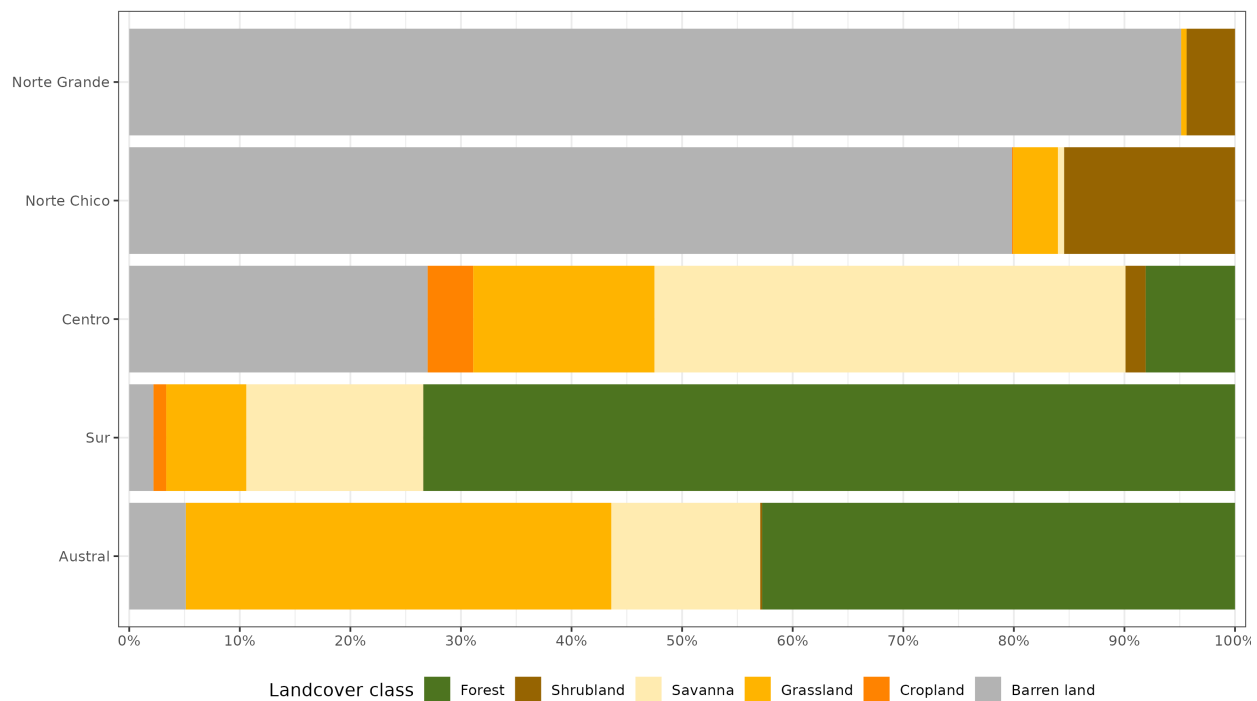


Figure 2: Proportion of land cover class from the persistent land cover for 2001-2022 (>80%) per macrozone

Table 3: The value of Sen's slope trend next to the time-series plot of surface per land cover class (IGBP MCD12Q1.016) for 2001–2022 through Central Chile. Values of zero indicate that there was not a significant trend. Red dots on the plots indicate the maximum and minimum values of surface.

macrozone	Trend of change [km ² year ⁻¹]											
	Forest		Cropland		Grassland		Savanna		Shrubland		Barren land	
	x	y	x	y	x	y	x	y	x	y	x	y
Norte Grande							0.0				0.0	
Norte Chico					-12.1		0.0		-70.0		0.0	111.2
Centro					-22.4		83.2		-136.2		146.0	22.9
Sur		396.6			37.8		0.0		-318.8		0.0	
Austral		0.0					0.0		172.1		-36.9	-93.2

291 Further, we want to address whether the trend in land cover change for 2001–2023 is associated with

292 trends in drought indices of water demand and supply and/or soil moisture for macrozone and land cover
 293 macroclasses. From the three methods tested, Ridge, Lasso, and Random Forest, neither gives significant
 294 results regarding whether the trend in a drought index for any time scale explains the trend in land cover
 295 change. Nevertheless, in “Norte Chico” and “Centro,” there is a decrease in croplands and savanna and an
 296 increase in barren land, which is associated with the variation in drought indices. Mainly for a decrease in
 297 water supply (SPI and SSI) and an increase in water demand (EDDI). However, due to the high variability
 298 from north to south in Chile, the climatic condition (arid, semi-arid, and humid), and the land cover type,
 299 we believe that only in those zones could the LULCC be driven to some degree by drought.

300 4.3. Trend of drought indices for water demand and supply, soil moisture, and vegetation productivity

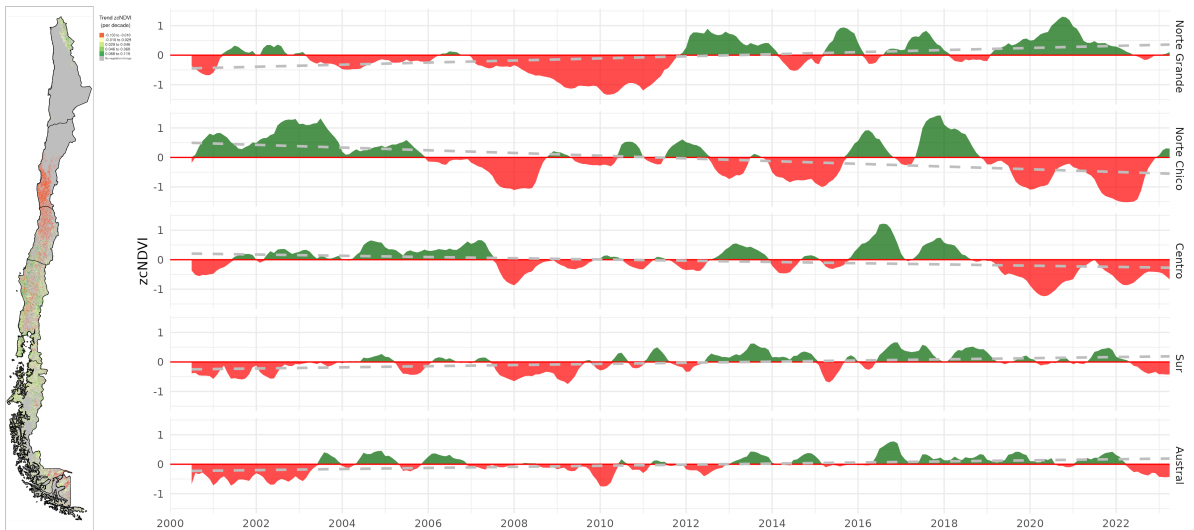


Figure 3: (a) Map of the linear trend of the index zcNDVI-6 for 2001–2023. Greener colors indicate a positive trend; red colors correspond to a negative trend and a decrease in vegetation productivity. Grey colors indicate either no vegetation or a change in land cover type for 2001–2022. (b) Temporal variation of zcNDVI-6 aggregated at macrozone level within continental Chile. Each horizontal panel corresponds to ‘Norte Grande’ to ‘Austral’.

301 Regarding vegetation productivity aggregated through the macrozones in the five land cover macroclasses,
 302 in “Norte Grande,” there is an increase trend of 0.02 (z-index) per decade, related to types of grassland
 303 and shrubland. There is a negative trend in “Norte Chico” with -0.04 and “Centro” with -0.02 per decade.
 304 In the “Norte Chico,” savanna (-0.05) has the lowest trend, and the rest of the types are around -0.04. In
 305 “Centro,” shrubland reaches -0.06, grassland -0.05, and croplands and savanna -0.01 per decade. This could
 306 be associated either with a reduction in vegetation surface, a decrease in biomass, or browning ([Miranda et al., 2023](#)). Vegetation reached its lowest values since the year 2019, reaching an extreme condition in early
 307 2020 and 2022 in the “Norte Chico” and “Centro” (Mega Drought). The “Sur” and “Austral” show a positive
 308 trend of around 0.016 per decade (Figure 3). Despite the croplands suffering from drought just as badly as
 309 the native vegetation in “Norte Chico,” the Chilean matorral appears to be the region most affected by a
 310 negative trend in vegetation ([Fuentes et al., 2021](#)).

312 Analyzing the water supply, the macrozones that have the lowest trend are “Norte Chico” and “Centro,”
 313 where the SPI, SPEI, and SSI show that it decreases at longer time scales due to the prolonged reduction in
 314 precipitation. At 36 months, it reaches trends between -0.03 and -0.04 (z-score) per decade for SPI, SPEI,
 315 and SSI (Figure 5). For “Sur,” the behavior is similar, decreasing at longer scales and having between -0.016
 316 and -0.025 per decade for SPI, SPEI, and SSI. On the other hand, all macrozones show an increase in the
 317 trend in all the drought indices, with “Norte Grande” having the highest at 36 months (0.042 per decade).
 318 Because of this, the SPEI (which uses AED) reached its lowest value in “Norte Grande,” with -0.03 at 36
 319 months. Despite the other macrozones, “Austral” showed an increase in all indices, being the highest for

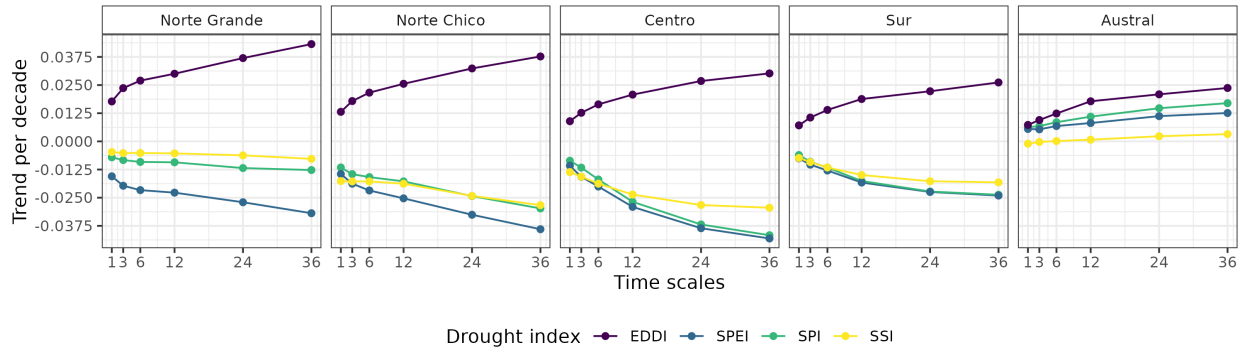


Figure 4: Trend per decade for the drought indices SPI, EDDI, SPEI, and SSI aggregated by macrozone.

320 EDDI at 36 months (0.025) and the lowest for SSI, which shows only a minor increase in the trend (Figure 5
 321 and Figure 4).

322 4.4. Impact for water supply and demand, and soil moisture in vegetation productivity

323 According to what is shown in Figure 6, Figure 7, and Table 4, forest seems to be the most resistant type
 324 to drought. Showing that only “Centro” is slightly ($rsq = 0.25$) impacted by a 12-month soil moisture deficit
 325 (SSI-12). In the “Norte Chico” and to a lesser extent in the “Norte Grande,” it is evident that a SSI-12 with
 326 a $rsq = 0.45$ and a decrease in water supply (SPI-36 and SPEI-24 with $rsq = 0.28$ and 0.34, respectively)
 327 have an impact on grasslands. However, this type was unaffected by soil moisture, water supply, or demand
 328 in macrozones further south. The types that show to be most affected by variation in climate conditions
 329 are shrublands, savannas, and croplands. For savannas in “Norte Chico,” the SSI-12 and SPI-24 reached
 330 an rsq of 0.74 and 0.58, respectively. This value decreases to the south, but the SSI-12 is still the variable
 331 explaining more of the variation in vegetation productivity ($rsq = 0.45$ in “Centro” and 0.2 in “Sur”). In
 332 the case of croplands, the SPEI-12, SPI-36, and SSI-12 explain between 45% and 66% of “Norte Chico.”
 333 The type of land most impacted by climatic variation was shrubland, where soil moisture explained 59%
 334 and precipitation, 37%, in “Norte Chico” and “Centro,” with SSI-12 being the most relevant variable, then
 335 SPI-36 in “Norte Chico” and SPI-24 in “Sur.”

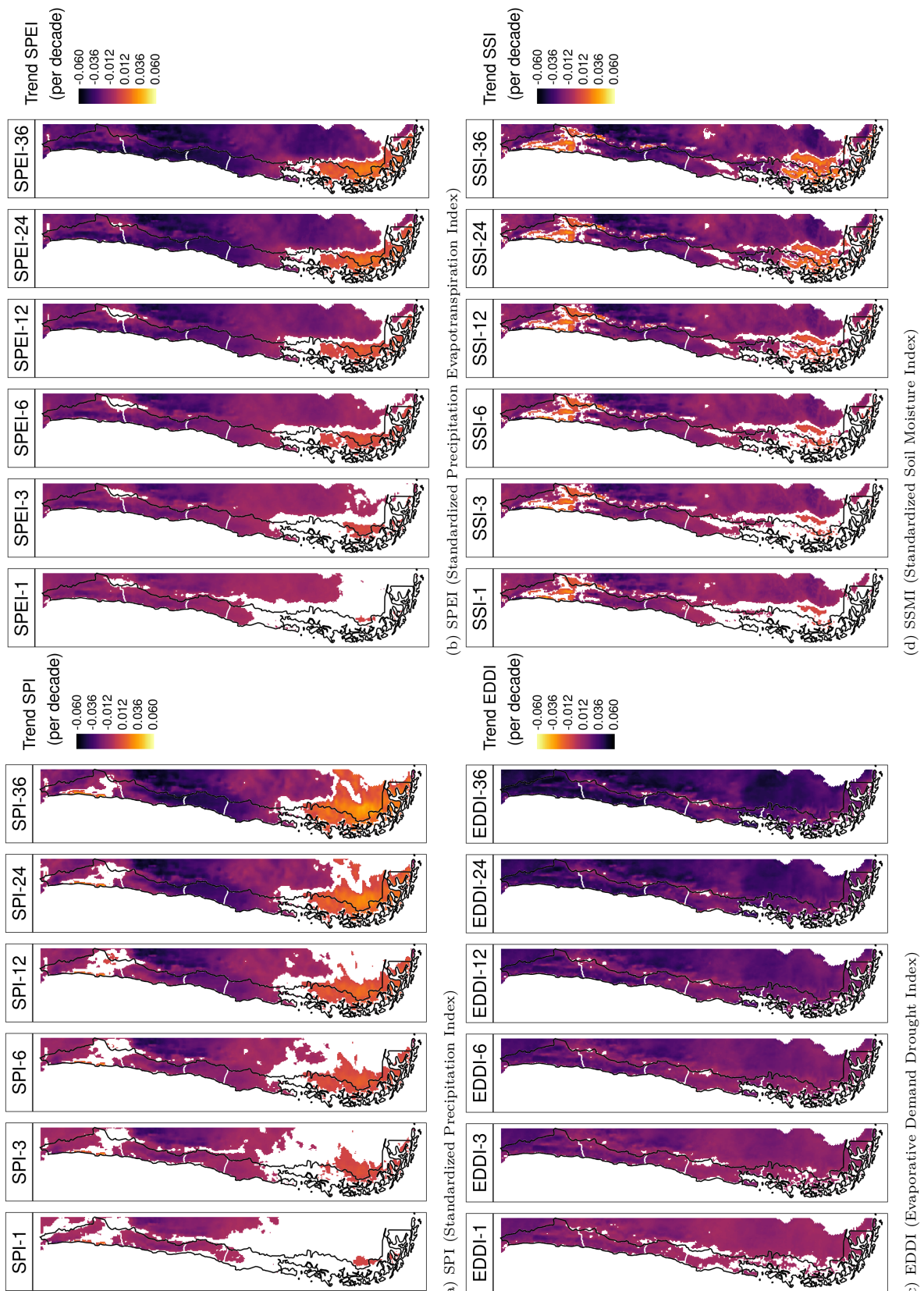
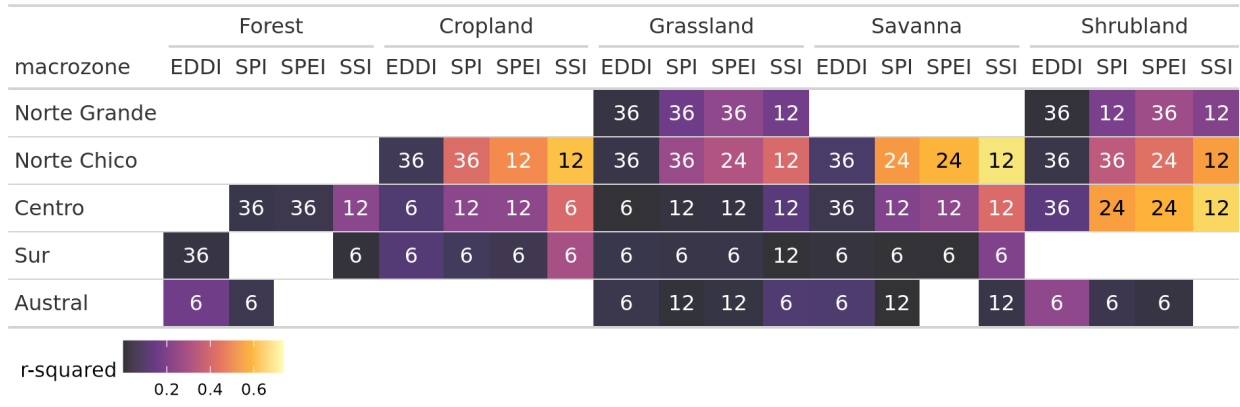


Figure 5: Linear trend of the drought index (*) at time scales of 1, 3, 6, 12, 24, and 36 months for 1981-2023

Table 4: Summary per land cover macroclass and macrozone regarding the correlation between zcNDVI with the drought indices EDDI, SPI, SPEI, and SSI for time scales of 1, 3, 6, 12, 24, and 36. The numbers in each cell indicate the time scale that reached the maximum correlation for the land cover and macrozone, and the color indicates the strength of the r-squared obtained with the index and the time scale.



336 5. Discussion

337 5.1. Drought trend, LULCC, and climate conditions

338 1.- Respecto a lo que indica [Vicente-Serrano et al. \(2018\)](#), de que el aumento en la tendencia en severidad
 339 de la sequía (hidrológica) tiene que ver más con un aumento de la demanda de agua (ej, LULCC, amazonas)
 340 que a una tendencia en las condiciones climáticas (SPI-12). ¿Qué pasa en Chile?

341 5.2. land cover types most impacted by drought throughout Chile

342 2.- Sobre los tipos de land cover más afectados por los indicadores de sequía. Asociación con el matorral
 343 chileno ([Fuentes et al., 2021](#)). Diferencia entre el Norte Chico, Centro y lo que pasa hacia el sur ([Miranda et al. \(2023\)](#))

345 5.3. Drought indices of water demand and supply, soil moisture to predict changes in vegetation productivity

346 3. Como podrían servir estos resultados para desarrollar o mejorar un predictor de productividad de la
 347 vegetación.

- 348 • Los datos ERA5L están casi en tiempo real, 7 días; MODIS también.
- 349 • EL SSI se ve como un poderoso indicador que explica la variabilidad en la productividad de la veg-
 350 etación.

351 5.4. Future outlook

352 4.- Qué se podría hacer mejor en futuras investigaciones del tema. - mejorar la resolución y calidad de los
 353 datos climáticos -

354 6. Conclusion

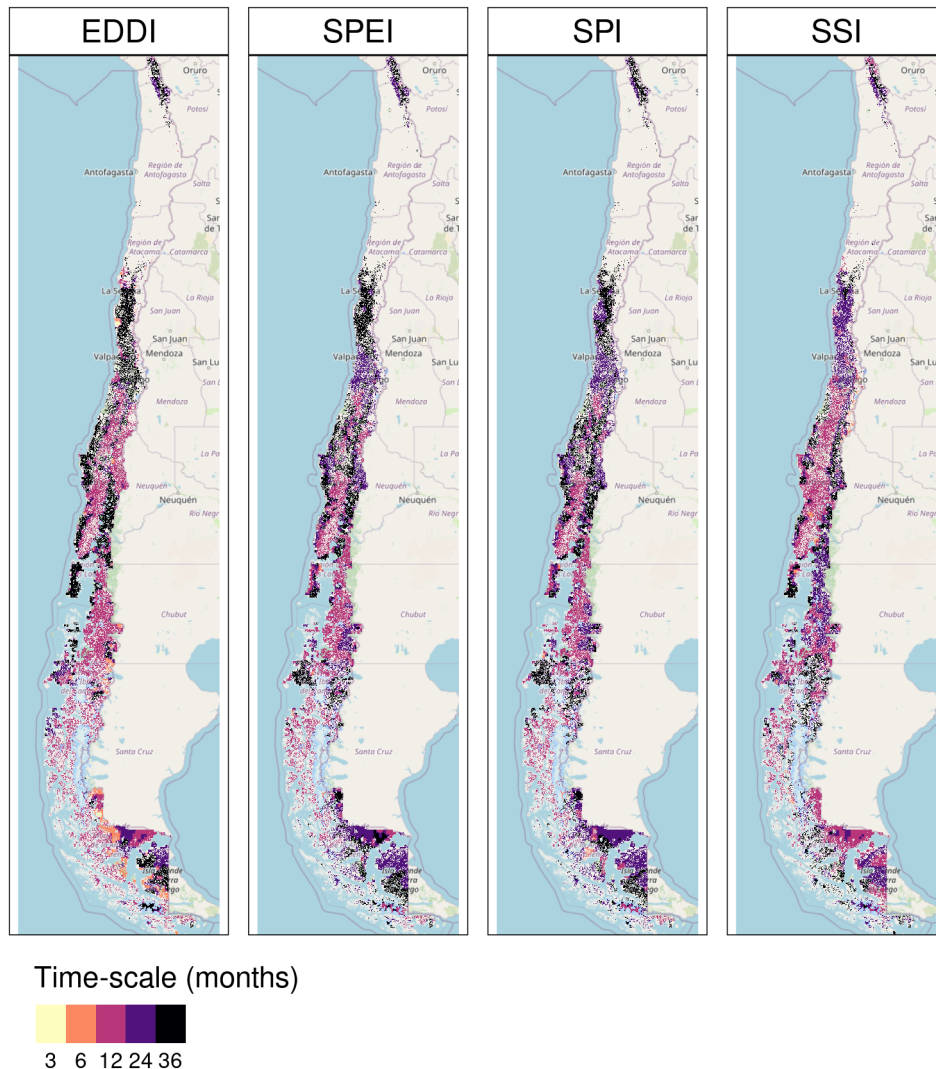


Figure 6: Time scales per drought index that reach the maximum coefficient of determination

References

- 355 Abramowitz, M., Stegun, I.A., 1968. Handbook of mathematical functions with formulas, graphs, and mathematical tables. volume 55. US Government printing office.
- 356 Aceituno, P., Boisier, J.P., Garreaud, R., Rondanelli, R., Rulltall, J.A., 2021. Climate and Weather in Chile, in: Fernández, B., Gironás, J. (Eds.), Water Resources of Chile. Springer International Publishing, Cham. volume 8, pp. 7–29. URL: http://link.springer.com/10.1007/978-3-030-56901-3_2.
- 361 AghaKouchak, A., 2014. A baseline probabilistic drought forecasting framework using standardized soil moisture index: application to the 2012 United States drought. *Hydrology and Earth System Sciences* 18, 2485–2492. URL: <https://hess.copernicus.org/articles/18/2485/2014/>, doi:[10.5194/hess-18-2485-2014](https://doi.org/10.5194/hess-18-2485-2014).
- 362 AghaKouchak, A., Farahmand, A., Melton, F.S., Teixeira, J., Anderson, M.C., Wardlow, B.D., Hain, C.R., 2015. Remote sensing of drought: Progress, challenges and opportunities. *Reviews of Geophysics* 53, 452–480. URL: <http://dx.doi.org/10.1002/2014RG000456>, doi:[10.1002/2014RG000456](https://doi.org/10.1002/2014RG000456).
- 363 AghaKouchak, A., Mirchi, A., Madani, K., Di Baldassarre, G., Nazemi, A., Alborzi, A., Anjileli, H., Azarderakhsh, M., Chiang, F., Hassanzadeh, E., Huning, L.S., Mallakpour, I., Martinez, A., Mazdiyasni, O., Moftakhar, H., Norouzi, H., Sadegh, M., Sadeqi, D., Van Loon, A.F., Wanders, N., 2021. Anthropogenic Drought: Definition, Challenges, and Opportunities. *Reviews of Geophysics* 59, e2019RG000683. URL: <https://agupubs.onlinelibrary.wiley.com/doi/10.1029/2019RG000683>, doi:[10.1029/2019RG000683](https://doi.org/10.1029/2019RG000683).
- 364 Ahmed, M., Sultan, M., Wahr, J., Yan, E., 2014. The use of GRACE data to monitor natural and anthropogenic induced

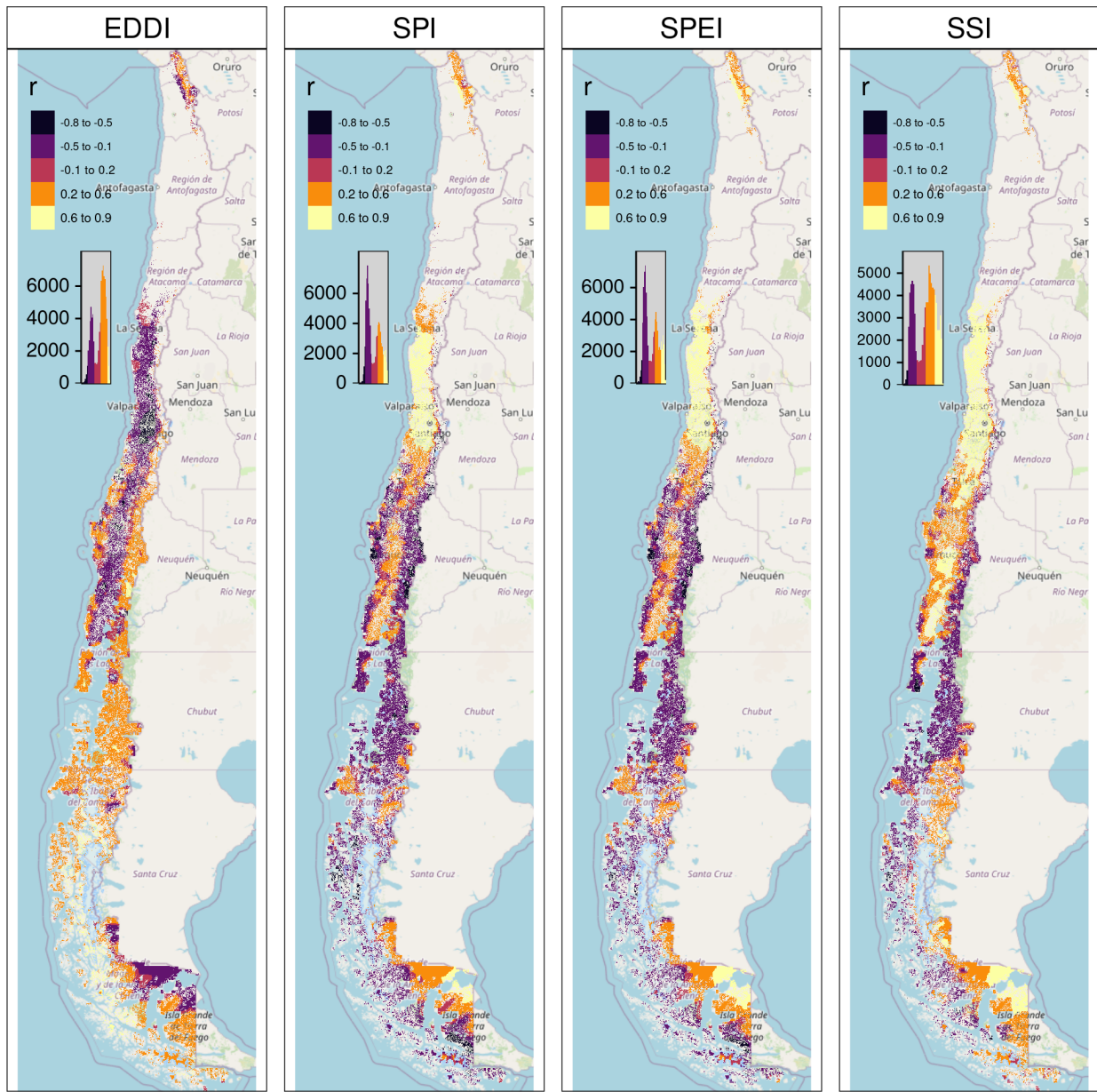


Figure 7: Pearson correlation value for the time scales and drought index that reach the maximum coefficient of determination

- variations in water availability across Africa. *Earth-Science Reviews* 136, 289–300. doi:[10.1016/J.EARSCIREV.2014.05.009](https://doi.org/10.1016/J.EARSCIREV.2014.05.009). publisher: Elsevier.
- Akinyemi, F.O., 2021. Vegetation Trends, Drought Severity and Land Use-Land Cover Change during the Growing Season in Semi-Arid Contexts. *Remote Sensing* 2021, Vol. 13, Page 836 13, 836. URL: <https://www.mdpi.com/2072-4292/13/5/836/>, doi:[10.3390/RS13050836](https://doi.org/10.3390/RS13050836). publisher: Multidisciplinary Digital Publishing Institute.
- Alvarez-Garreton, C., Boisier, J.P., Garreaud, R., Seibert, J., Vis, M., 2021. Progressive water deficits during multiyear droughts in basins with long hydrological memory in Chile. *Hydrology and Earth System Sciences* 25, 429–446. URL: <https://hess.copernicus.org/articles/25/429/2021/>, doi:[10.5194/hess-25-429-2021](https://doi.org/10.5194/hess-25-429-2021).
- Beck, H.E., McVicar, T.R., Vergopolan, N., Berg, A., Lutsko, N.J., Dufour, A., Zeng, Z., Jiang, X., van Dijk, A.I.J.M., Miralles, D.G., 2023. High-resolution (1 km) Köppen-Geiger maps for 1901–2099 based on constrained CMIP6 projections. *Scientific Data* 10. URL: <http://dx.doi.org/10.1038/s41597-023-02549-6>, doi:[10.1038/s41597-023-02549-6](https://doi.org/10.1038/s41597-023-02549-6).
- Beguería, S., Vicente-Serrano, S.M., 2023. SPEI: Calculation of the Standardized Precipitation-Evapotranspiration Index. URL:

- 385 <https://CRAN.R-project.org/package=SPEI>.
- 386 Boisier, J.P., Alvarez-Garreton, C., Cordero, R.R., Damiani, A., Gallardo, L., Garreaud, R.D., Lambert, F., Ramallo, C.,
 387 Rojas, M., Rondanelli, R., 2018. Anthropogenic drying in central-southern Chile evidenced by long-term observations
 388 and climate model simulations. *Elementa* 6, 74. URL: <https://www.elementascience.org/article/10.1525/elementa.328/>,
 389 doi:[10.1525/elementa.328](https://doi.org/10.1525/elementa.328).
- 390 Calvin, K., Dasgupta, D., Krinner, G., Mukherji, A., Thorne, P.W., Trisos, C., Romero, J., Aldunce, P., Barrett, K., Blanco,
 391 G., Cheung, W.W., Connors, S., Denton, F., Diongue-Niang, A., Dodman, D., Garschagen, M., Geden, O., Hayward, B.,
 392 Jones, C., Jotzo, F., Krug, T., Lasco, R., Lee, Y.Y., Masson-Delmotte, V., Meinshausen, M., Mintenbeck, K., Mokssit, A.,
 393 Otto, F.E., Pathak, M., Pirani, A., Poloczanska, E., Pörtner, H.O., Revi, A., Roberts, D.C., Roy, J., Ruane, A.C., Skea,
 394 J., Shukla, P.R., Slade, R., Slangen, A., Sokona, Y., Sörensson, A.A., Tignor, M., Van Vuuren, D., Wei, Y.M., Winkler,
 395 H., Zhai, P., Zommers, Z., Hourcade, J.C., Johnson, F.X., Pachauri, S., Simpson, N.P., Singh, C., Thomas, A., Totin, E.,
 396 Arias, P., Bustamante, M., Elgizouli, I., Flato, G., Howden, M., Méndez-Vallejo, C., Pereira, J.J., Pichs-Madruga, R., Rose,
 397 S.K., Saheb, Y., Sánchez Rodríguez, R., Ürge Vorsatz, D., Xiao, C., Yassa, N., Alegría, A., Armour, K., Bednar-Friedl, B.,
 398 Blok, K., Cissé, G., Dentener, F., Eriksen, S., Fischer, E., Garner, G., Guivarc, C., Haasnoot, M., Hansen, G., Hauser, M.,
 399 Hawkins, E., Hermans, T., Kopp, R., Leprince-Ringuet, N., Lewis, J., Ley, D., Ludden, C., Niamir, L., Nicholls, Z., Some,
 400 S., Szopa, S., Trewhin, B., Van Der Wijst, K.I., Winter, G., Witting, M., Birt, A., Ha, M., Romero, J., Kim, J., Haites, E.F.,
 401 Jung, Y., Stavins, R., Birt, A., Ha, M., Orendain, D.J.A., Ignon, L., Park, S., Park, Y., Reisinger, A., Cammaramo, D.,
 402 Fischlin, A., Fuglestvedt, J.S., Hansen, G., Ludden, C., Masson-Delmotte, V., Matthews, J.R., Mintenbeck, K., Pirani, A.,
 403 Poloczanska, E., Leprince-Ringuet, N., Péan, C., 2023. IPCC, 2023: Climate Change 2023: Synthesis Report. Contribution
 404 of Working Groups I, II and III to the Sixth Assessment Report of the Intergovernmental Panel on Climate Change [Core
 405 Writing Team, H. Lee and J. Romero (eds.)]. IPCC, Geneva, Switzerland. Technical Report. Intergovernmental Panel on
 406 Climate Change (IPCC). URL: <https://www.ipcc.ch/report/ar6/syr/>.
- 407 Crausbay, S.D., Ramirez, A.R., Carter, S.L., Cross, M.S., Hall, K.R., Bathke, D.J., Betancourt, J.L., Colt, S., Cravens, A.E.,
 408 Dalton, M.S., Dunham, J.B., Hay, L.E., Hayes, M.J., McEvoy, J., McNutt, C.A., Moritz, M.A., Nislow, K.H., Raheem, N.,
 409 Sanford, T., 2017. Defining Ecological Drought for the Twenty-First Century. *Bulletin of the American Meteorological Society*
 410 98, 2543–2550. URL: <https://journals.ametsoc.org/view/journals/bams/98/12/bams-d-16-0292.1.xml>, doi:[10.1175/BAMS-D-16-0292.1](https://doi.org/10.1175/BAMS-D-16-0292.1). publisher: American Meteorological Society.
- 411 Cui, A., Li, J., Zhou, Q., Zhu, R., Liu, H., Wu, G., Li, Q., 2021. Use of a multiscalar GRACE-based standardized terrestrial
 412 water storage index for assessing global hydrological droughts. *Journal of Hydrology* 603, 126871. URL: <https://linkinghub.elsevier.com/retrieve/pii/S0022169421009215>, doi:[10.1016/j.jhydrol.2021.126871](https://doi.org/10.1016/j.jhydrol.2021.126871).
- 412 Didan, K., 2015. MOD13Q1 MODIS/Terra Vegetation Indices 16-Day L3 Global 250m SIN Grid V006. Technical Report.
 413 NASA EOSDIS Land Processes DAAC. doi:<http://dx.doi.org/10.5067/MODIS/MOD13Q1.006>.
- 414 Fernández, F.J., Vásquez-Lavín, F., Ponce, R.D., Garreaud, R., Hernández, F., Link, O., Zambrano, F., Hanemann, M., 2023.
 415 The economics impacts of long-run droughts: Challenges, gaps, and way forward. *Journal of Environmental Management*
 416 344, 118726. URL: <https://linkinghub.elsevier.com/retrieve/pii/S0301479723015141>, doi:[10.1016/j.jenvman.2023.118726](https://doi.org/10.1016/j.jenvman.2023.118726).
- 417 Friedl, M., Sulla-Menashe, D., 2019. MCD12Q1 MODIS/Terra+Aqua Land Cover Type Yearly L3 Global 500m SIN Grid V006
 418 [Data set]. NASA EOSDIS Land Processes DAAC. doi:[10.5067/MODIS/MCD12Q1.006](http://dx.doi.org/10.5067/MODIS/MCD12Q1.006).
- 419 Fuentes, I., Fuster, R., Avilés, D., Vervoort, W., 2021. Water scarcity in central Chile: the effect of climate and land cover
 420 changes on hydrologic resources. *Hydrological Sciences Journal* 66, 1028–1044. URL: <https://www.tandfonline.com/doi/full/10.1080/02626667.2021.1903475>, doi:[10.1080/02626667.2021.1903475](https://doi.org/10.1080/02626667.2021.1903475).
- 421 Garreaud, R., Alvarez-Garreton, C., Barichivich, J., Boisier, J.P., Christie, D., Galleguillos, M., LeQuenne, C., McPhee, J.,
 422 Zambrano-Bigiarini, M., 2017. The 2010–2015 mega drought in Central Chile: Impacts on regional hydroclimate and
 423 vegetation. *Hydrology and Earth System Sciences Discussions* 2017, 1–37. URL: <http://www.hydrol-earth-syst-sci-discuss.net/hess-2017-191/>, doi:[10.5194/hess-2017-191](https://doi.org/10.5194/hess-2017-191).
- 424 Garreaud, R.D., 2009. The Andes climate and weather. *Advances in Geosciences* 22, 3–11. URL: <https://adgeo.copernicus.org/articles/22/3/2009/>, doi:[10.5194/adgeo-22-3-2009](https://doi.org/10.5194/adgeo-22-3-2009).
- 425 Garreaud, R.D., Boisier, J.P., Rondanelli, R., Montecinos, A., Sepúlveda, H.H., Veloso-Aguila, D., 2020. The Central Chile
 426 Mega Drought (2010–2018): A climate dynamics perspective. *International Journal of Climatology* 40, 421–439. URL:
 427 <https://rmets.onlinelibrary.wiley.com/doi/10.1002/joc.6219>, doi:[10.1002/joc.6219](https://doi.org/10.1002/joc.6219).
- 428 Grekousis, G., Mountrakis, G., Kavouras, M., 2015. An overview of 21 global and 43 regional land-cover mapping products.
 429 *International Journal of Remote Sensing* 36, 5309–5335. URL: <https://www.tandfonline.com/doi/full/10.1080/01431161.2015.1093195>, doi:[10.1080/01431161.2015.1093195](https://doi.org/10.1080/01431161.2015.1093195).
- 430 Hao, Z., AghaKouchak, A., 2013. Multivariate Standardized Drought Index: A parametric multi-index model. *Advances in Water
 431 Resources* 57, 12–18. URL: <https://linkinghub.elsevier.com/retrieve/pii/S0309170813000493>, doi:[10.1016/j.advwatres.2013.03.009](https://doi.org/10.1016/j.advwatres.2013.03.009).
- 431 Hargreaves, G.H., 1994. Defining and Using Reference Evapotranspiration. *Journal of Irrigation and Drainage Engineering* 120,
 432 1132–1139. URL: <https://ascelibrary.org/doi/10.1061/%28ASCE%290733-9437%281994%29120%3A6%281132%29>, doi:[10.1061/\(ASCE\)0733-9437\(1994\)120:6\(1132\)](https://doi.org/10.1061/(ASCE)0733-9437(1994)120:6(1132)).
- 432 Hargreaves, G.H., Samani, Z.A., 1985. Reference crop evapotranspiration from temperature. *Applied engineering in agriculture*
 433 1, 96–99.
- 434 Hijmans, R.J., 2023. terra: Spatial Data Analysis. URL: <https://CRAN.R-project.org/package=terra>.
- 435 Ho, T.K., 1995. Random decision forests, in: *Proceedings of 3rd international conference on document analysis and recognition*,
 436 IEEE. pp. 278–282.
- 437 Hobbins, M.T., Wood, A., McEvoy, D.J., Huntington, J.L., Morton, C., Anderson, M., Hain, C., 2016. The Evaporative Demand
 438 Drought Index. Part I: Linking Drought Evolution to Variations in Evaporative Demand. *Journal of Hydrometeorology* 17,

- 450 1745–1761. URL: <http://journals.ametsoc.org/doi/10.1175/JHM-D-15-0121.1>, doi:[10.1175/JHM-D-15-0121.1](https://doi.org/10.1175/JHM-D-15-0121.1).
- 451 Hoerl, A.E., Kennard, R.W., 1970. Ridge Regression: Biased Estimation for Nonorthogonal Problems. *Technometrics* 12, 55–67.
- 452 URL: <http://www.tandfonline.com/doi/abs/10.1080/00401706.1970.10488634>, doi:[10.1080/00401706.1970.10488634](https://doi.org/10.1080/00401706.1970.10488634).
- 453 Hufkens, K., Stauffer, R., Campitelli, E., 2019. The ecwmfr package: an interface to ECMWF API endpoints. URL: <https://bluegreen-labs.github.io/ecmwfr/>.
- 454 IPCC, 2013. Climate Change 2013: The Physical Science Basis. Contribution of Working Group I to the Fifth Assessment Report of the Intergovernmental Panel on Climate Change. Cambridge University Press, Cambridge, UK; New York, USA.
- 455 URL: www.climatechange2013.org, doi:[10.1017/CBO9781107415324](https://doi.org/10.1017/CBO9781107415324).
- 456 Kendall, M., 1975. Rank correlation methods (4th ed. 2d impression). Griffin.
- 457 Kogan, F.N., 1995. Application of vegetation index and brightness temperature for drought detection. *Advances in Space Research* 15, 91–100. doi:[10.1016/0273-1177\(95\)00079-T](https://doi.org/10.1016/0273-1177(95)00079-T).
- 458 Luo, L., Apps, D., Arcand, S., Xu, H., Pan, M., Hoerling, M., 2017. Contribution of temperature and precipitation anomalies to the California drought during 2012–2015. *Geophysical Research Letters* 44, 3184–3192. URL: <https://agupubs.onlinelibrary.wiley.com/doi/10.1002/2016GL072027>, doi:[10.1002/2016GL072027](https://doi.org/10.1002/2016GL072027).
- 459 Ma, S., Wu, Q., Wang, J., Zhang, S., 2017. Temporal Evolution of Regional Drought Detected from GRACE TWSA and CCI SM in Yunnan Province, China. *Remote Sensing* 2017, Vol. 9, Page 1124 9, 1124. URL: <https://www.mdpi.com/2072-4292/9/11/1124/htm>, doi:[10.3390/RS9111124](https://doi.org/10.3390/RS9111124). publisher: Multidisciplinary Digital Publishing Institute.
- 460 McEvoy, D.J., Huntington, J.L., Hobbins, M.T., Wood, A., Morton, C., Anderson, M., Hain, C., 2016. The Evaporative Demand Drought Index. Part II: CONUS-Wide Assessment against Common Drought Indicators. *Journal of Hydrometeorology* 17, 1763–1779. URL: <http://journals.ametsoc.org/doi/10.1175/JHM-D-15-0122.1>, doi:[10.1175/JHM-D-15-0122.1](https://doi.org/10.1175/JHM-D-15-0122.1).
- 461 McKee, T.B., Doesken, N.J., Kleist, J., 1993. The relationship of drought frequency and duration to time scales. In: Proceedings of the Ninth Conference on Applied Climatology. American Metereological Society , 179–184.
- 462 Meroni, M., Rembold, F., Fasbender, D., Vrieling, A., 2017. Evaluation of the Standardized Precipitation Index as an early predictor of seasonal vegetation production anomalies in the Sahel. *Remote Sensing Letters* 8, 301–310. URL: <https://www.tandfonline.com/doi/full/10.1080/2150704X.2016.1264020>, doi:[10.1080/2150704X.2016.1264020](https://doi.org/10.1080/2150704X.2016.1264020).
- 463 Miranda, A., Lara, A., Altamirano, A., Di Bella, C., González, M.E., Julio Camarero, J., 2020. Forest browning trends in response to drought in a highly threatened mediterranean landscape of South America. *Ecological Indicators* 115, 106401. URL: <https://linkinghub.elsevier.com/retrieve/pii/S1470160X20303381>, doi:[10.1016/j.ecolind.2020.106401](https://doi.org/10.1016/j.ecolind.2020.106401).
- 464 Miranda, A., Syphard, A.D., Berdugo, M., Carrasco, J., Gómez-González, S., Ovalle, J.F., Delpiano, C.A., Vargas, S., Squeo, F.A., Miranda, M.D., Dobbs, C., Mentler, R., Lara, A., Garreaud, R., 2023. Widespread synchronous decline of Mediterranean-type forest driven by accelerated aridity. *Nature Plants* 9, 1810–1817. URL: <https://www.nature.com/articles/s41477-023-01541-7>, doi:[10.1038/s41477-023-01541-7](https://doi.org/10.1038/s41477-023-01541-7).
- 465 Muñoz-Sabater, J., Dutra, E., Agustí-Panareda, A., Albergel, C., Arduini, G., Balsamo, G., Boussetta, S., Choulga, M., Harrigan, S., Hersbach, H., Martens, B., Miralles, D.G., Piles, M., Rodríguez-Fernández, N.J., Zsoter, E., Buontempo, C., Thépaut, J.N., 2021. ERA5-Land: a state-of-the-art global reanalysis dataset for land applications. *Earth System Science Data* 13, 4349–4383. URL: <https://essd.copernicus.org/articles/13/4349/2021/>, doi:[10.5194/essd-13-4349-2021](https://doi.org/10.5194/essd-13-4349-2021).
- 466 Narasimhan, B., Srinivasan, R., 2005. Development and evaluation of Soil Moisture Deficit Index (SMDI) and Evapotranspiration Deficit Index (ETDI) for agricultural drought monitoring. *Agricultural and Forest Meteorology* 133, 69–88. URL: <https://linkinghub.elsevier.com/retrieve/pii/S0168192305001565>, doi:[10.1016/j.agrformet.2005.07.012](https://doi.org/10.1016/j.agrformet.2005.07.012).
- 467 Nouri, M., 2023. Drought Assessment Using Gridded Data Sources in Data-Poor Areas with Different Aridity Conditions. *Water Resources Management* 37, 4327–4343. URL: <https://link.springer.com/10.1007/s11269-023-03555-4>, doi:[10.1007/s11269-023-03555-4](https://doi.org/10.1007/s11269-023-03555-4).
- 468 Paruelo, J.M., Texeira, M., Staiano, L., Mastrángelo, M., Amdan, L., Gallego, F., 2016. An integrative index of Ecosystem Services provision based on remotely sensed data. *Ecological Indicators* 71, 145–154. URL: <https://www.sciencedirect.com/science/article/pii/S1470160X16303843>, doi:[10.1016/J.ECOLIND.2016.06.054](https://doi.org/10.1016/J.ECOLIND.2016.06.054). publisher: Elsevier.
- 469 Pebesma, E., 2018. Simple Features for R: Standardized Support for Spatial Vector Data. *The R Journal* 10, 439–446. URL: <https://doi.org/10.32614/RJ-2018-009>, doi:[10.32614/RJ-2018-009](https://doi.org/10.32614/RJ-2018-009).
- 470 Pebesma, E., Bivand, R., 2023. Spatial Data Science: With applications in R. Chapman and Hall/CRC, London. URL: <https://r-spatial.org/book/>.
- 471 R Core Team, 2023. R: A Language and Environment for Statistical Computing. R Foundation for Statistical Computing, Vienna, Austria. URL: <https://www.R-project.org/>.
- 472 Schucknecht, A., Meroni, M., Kayitakire, F., Boureima, A., Schucknecht, A., Meroni, M., Kayitakire, F., Boureima, A., 2017. Phenology-Based Biomass Estimation to Support Rangeland Management in Semi-Arid Environments. *Remote Sensing* 9, 463. URL: <https://www.mdpi.com/2072-4292/9/5/463>, doi:[10.3390/rs9050463](https://doi.org/10.3390/rs9050463). publisher: Multidisciplinary Digital Publishing Institute.
- 473 Sen, P.K., 1968. Estimates of the Regression Coefficient Based on Kendall's Tau. *Journal of the American Statistical Association* 63, 1379–1389. URL: <http://www.tandfonline.com/doi/abs/10.1080/01621459.1968.10480934>, doi:[10.1080/01621459.1968.10480934](https://doi.org/10.1080/01621459.1968.10480934).
- 474 Seneviratne, S and Zhang, X.a.A.M.a.B.W.a.D.C.a.L.A.a.G.S.a.I.I.a.K.J.a.L.S.a.O.F.a.P.I.a.S.M.a.V.S.S.a.W.M.a.Z..M.D.B.a.V.a.O., 2021. Weather and Climate Extreme Events in a Changing Climate. Cambridge University Press. In Press. Publication Title: Climate Change 2021: The Physical Science Basis. Contribution of Working Group I to the Sixth Assessment Report of the Intergovernmental Panel on Climate Change.
- 475 Slette, I.J., Post, A.K., Awad, M., Even, T., Punzalan, A., Williams, S., Smith, M.D., Knapp, A.K., 2019. How ecologists define drought, and why we should do better. *Global Change Biology* 25, 3193–3200. URL: <https://onlinelibrary.wiley.com/doi/10.1111/gcb.14747>, doi:[10.1111/gcb.14747](https://doi.org/10.1111/gcb.14747).

- 515 Souza, A.G.S.S., Ribeiro Neto, A., Souza, L.L.D., 2021. Soil moisture-based index for agricultural drought assessment: SMADI
 516 application in Pernambuco State-Brazil. *Remote Sensing of Environment* 252, 112124. URL: <https://linkinghub.elsevier.com/retrieve/pii/S0034425720304971>, doi:[10.1016/j.rse.2020.112124](https://doi.org/10.1016/j.rse.2020.112124).
- 517 Tibshirani, R., Bien, J., Friedman, J., Hastie, T., Simon, N., Taylor, J., Tibshirani, R.J., 2010. Strong rules for discarding
 518 predictors in lasso-type problems. URL: <http://arxiv.org/abs/1011.2234>.
- 519 Tran, H.T., Campbell, J.B., Wynne, R.H., Shao, Y., Phan, S.V., 2019. Drought and Human Impacts on Land Use and Land
 520 Cover Change in a Vietnamese Coastal Area. *Remote Sensing* 2019, Vol. 11, Page 333 11, 333. URL: <https://www.mdpi.com/2072-4292/11/3/333/htm>, doi:[10.3390/RS11030333](https://doi.org/10.3390/RS11030333). publisher: Multidisciplinary Digital Publishing Institute.
- 521 Urrutia-Jalabert, R., González, M.E., González-Reyes, ., Lara, A., Garreaud, R., 2018. Climate variability and forest fires in
 522 central and south-central Chile. *Ecosphere* 9, e02171. URL: <https://esajournals.onlinelibrary.wiley.com/doi/10.1002/ecs2.2171>, doi:[10.1002/ecs2.2171](https://doi.org/10.1002/ecs2.2171).
- 523 Van Loon, A.F., Gleeson, T., Clark, J., Van Dijk, A.I., Stahl, K., Hannaford, J., Di Baldassarre, G., Teuling, A.J., Tallaksen,
 524 L.M., Uijlenhoet, R., Hannah, D.M., Sheffield, J., Svoboda, M., Verbeiren, B., Wagener, T., Rangecroft, S., Wanders, N.,
 525 Van Lanen, H.A., 2016. Drought in the Anthropocene. *Nature Geoscience* 9, 89–91. doi:[10.1038/ngeo2646](https://doi.org/10.1038/ngeo2646).
- 526 Venegas-González, A., Juñent, F.R., Gutiérrez, A.G., Filho, M.T., 2018. Recent radial growth decline in response to increased
 527 drought conditions in the northernmost Nothofagus populations from South America. *Forest Ecology and Management* 409,
 528 94–104. URL: <https://linkinghub.elsevier.com/retrieve/pii/S0378112717313993>, doi:[10.1016/j.foreco.2017.11.006](https://doi.org/10.1016/j.foreco.2017.11.006).
- 529 Vicente-Serrano, S.M., Azorin-Molina, C., Sanchez-Lorenzo, A., Revuelto, J., López-Moreno, J.I., González-Hidalgo, J.C.,
 530 Moran-Tejeda, E., Espejo, F., 2014. Reference evapotranspiration variability and trends in Spain, 1961–2011. *Global
 531 and Planetary Change* 121, 26–40. URL: <https://linkinghub.elsevier.com/retrieve/pii/S0921818114001180>, doi:[10.1016/j.gloplacha.2014.06.005](https://doi.org/10.1016/j.gloplacha.2014.06.005).
- 532 Vicente-Serrano, S.M., Beguería, S., López-Moreno, J.I., 2010. A multiscalar drought index sensitive to global warming: The
 533 standardized precipitation evapotranspiration index. *Journal of Climate* 23, 1696–1718. URL: <http://dx.doi.org/10.1175/2009JCLI2909.1>, doi:[10.1175/2009JCLI2909.1](https://doi.org/10.1175/2009JCLI2909.1).
- 534 Vicente-Serrano, S.M., Miralles, D.G., Domínguez-Castro, F., Azorin-Molina, C., El Kenawy, A., McVicar, T.R., Tomás-
 535 Burguera, M., Beguería, S., Maneta, M., Peña-Gallardo, M., 2018. Global Assessment of the Standardized Evapotranspiration
 536 Deficit Index (SEDI) for Drought Analysis and Monitoring. *Journal of Climate* 31, 5371–5393. URL: <https://journals.ametsoc.org/doi/10.1175/JCLI-D-17-0775.1>, doi:[10.1175/JCLI-D-17-0775.1](https://doi.org/10.1175/JCLI-D-17-0775.1).
- 537 Vicente-Serrano, S.M., Peña-Angulo, D., Beguería, S., Domínguez-Castro, F., Tomás-Burguera, M., Noguera, I., Gimeno-Sotelo,
 538 L., El Kenawy, A., 2022. Global drought trends and future projections. *Philosophical Transactions of the Royal Society A: Mathematical, Physical and Engineering Sciences* 380, 20210285. URL: <https://royalsocietypublishing.org/doi/10.1098/rsta.2021.0285>, doi:[10.1098/rsta.2021.0285](https://doi.org/10.1098/rsta.2021.0285).
- 539 Wang, M., Menzel, L., Jiang, S., Ren, L., Xu, C.Y., Cui, H., 2023. Evaluation of flash drought under the impact of heat wave
 540 events in southwestern Germany. *Science of The Total Environment* 904, 166815. URL: <https://linkinghub.elsevier.com/retrieve/pii/S0048969723054402>, doi:[10.1016/j.scitotenv.2023.166815](https://doi.org/10.1016/j.scitotenv.2023.166815).
- 541 West, H., Quinn, N., Horswell, M., 2019. Remote sensing for drought monitoring \& impact assessment: Progress, past
 542 challenges and future opportunities. *Remote Sensing of Environment* 232. doi:[10.1016/j.rse.2019.111291](https://doi.org/10.1016/j.rse.2019.111291). publisher:
 543 Elsevier Inc.
- 544 Wilhite, D.A., Glantz, M.H., 1985. Understanding: The drought phenomenon: The role of definitions. *Water International* 10,
 545 111–120. URL: <http://dx.doi.org/10.1080/02508068508686328>, doi:[10.1080/02508068508686328](https://doi.org/10.1080/02508068508686328).
- 546 Wilks, D.S., 2011. Empirical distributions and exploratory data analysis. *Statistical Methods in the Atmospheric Sciences* 100.
- 547 WMO, Svoboda, M., Hayes, M., Wood, D.A., 2012. Standardized Precipitation Index User Guide. WMO, Geneva. URL:
 548 http://library.wmo.int/opac/index.php?lvl=notice_display&id=13682. series Title: WMO Publication Title: WMO-No.
 549 1090 © Issue: 1090.
- 550 Zambrano, F., 2023. Four decades of satellite data for agricultural drought monitoring throughout the growing season in Central
 551 Chile, in: Vijay P. Singh Deepak Jhajharia, R.M., Kumar, R. (Eds.), *Integrated Drought Management*, Two Volume Set.
 552 CRC Press, p. 28.
- 553 Zambrano, F., Lillo-Saavedra, M., Verbist, K., Lagos, O., 2016. Sixteen years of agricultural drought assessment of the
 554 biobío region in chile using a 250 m resolution vegetation condition index (VCI). *Remote Sensing* 8, 1–20. URL: <https://www.mdpi.com/2072-4292/8/6/530>, doi:[10.3390/rs8060530](https://doi.org/10.3390/rs8060530). publisher: Multidisciplinary Digital Publishing Institute.
- 555 Zambrano, F., Vrieling, A., Nelson, A., Meroni, M., Tadesse, T., 2018. Prediction of drought-induced reduction of agricultural
 556 productivity in Chile from MODIS, rainfall estimates, and climate oscillation indices. *Remote Sensing of Environment*
 557 219, 15–30. URL: <https://www.sciencedirect.com/science/article/pii/S0034425718304541>, doi:[10.1016/j.rse.2018.10.006](https://doi.org/10.1016/j.rse.2018.10.006).
 558 publisher: Elsevier.
- 559 Zhao, Y., Feng, D., Yu, L., Wang, X., Chen, Y., Bai, Y., Hernández, H.J., Galleguillos, M., Estades, C., Biging, G.S., Radke,
 560 J.D., Gong, P., 2016. Detailed dynamic land cover mapping of Chile: Accuracy improvement by integrating multi-temporal
 561 data. *Remote Sensing of Environment* 183, 170–185. URL: <https://linkinghub.elsevier.com/retrieve/pii/S0034425716302188>,
 562 doi:[10.1016/j.rse.2016.05.016](https://doi.org/10.1016/j.rse.2016.05.016).